

Landau levels from neutral Bogoliubov particles in two-dimensional nodal superconductors under strain and doping gradients

Emilian M. Nica* and Marcel Franz

Department of Physics and Astronomy and Quantum Materials Institute,
University of British Columbia, Vancouver, B.C., V6T 1Z1, Canada

(Dated: April 28, 2022)

Motivated by recent work on strain-induced pseudo-magnetic fields in Dirac and Weyl semimetals, we analyze the possibility of analogous fields in two-dimensional nodal superconductors. We consider the prototypical case of a d -wave superconductor, a representative of the cuprate family, and find that the presence of weak strain leads to pseudo-magnetic fields and Landau quantization of Bogoliubov quasiparticles in the low-energy sector. A similar effect is induced by the presence of generic, weak doping gradients. In contrast to genuine magnetic fields in superconductors, the strain- and doping gradient-induced pseudo-magnetic fields couple in a way that preserves time-reversal symmetry and is not subject to the screening associated with the Meissner effect. These effects can be probed by tuning weak applied supercurrents which lead to shifts in the energies of the Landau levels and hence to quantum oscillations in thermodynamic and transport quantities.

Introduction.— Elementary excitations in superconductors are comprised of coherent superpositions of electron and hole degrees of freedom [1–3]. These Bogoliubov quasiparticles are electrically neutral on average and therefore do not couple simply to the externally applied magnetic field. In addition, superconductors are known to expel magnetic field from their bulk either completely [4], or form a flux lattice [5], in which the quasiparticle dynamics is effectively zero-field [6]. For these reasons superconductors normally avoid formation of Landau levels which represent the canonical response of most other electron systems to magnetic field [7].

In this work, we show that weak, in-plane strains and doping gradients generically lead to Landau quantization of Bogoliubov quasiparticles for a broad class of 2D nodal superconductors (SC). In these cases, the Dirac-like quasiparticles in the vicinity of point nodes are subject to emergent vector potentials which enter in a time-reversal invariant way. In contrast to genuine magnetic fields in a SC, there are no induced currents and no screening associated with the Meissner effect. Our work is motivated by interesting developments in graphene [8] where strain-induced pseudo-magnetic fields lead to Landau quantization and quantum oscillations, which were already observed in experiment [9], and more recent proposals in the context of Dirac and Weyl semimetals [10–15].

A possible experimental setup is shown in Fig. 1. Since the most immediate realization of gapless, effectively two-dimensional superconductivity is provided by the broad class of Cu-based materials, we study the case of a prototypical d -wave SC. Strain can be induced in principle by allowing for the controlled deformation of an underlying substrate [16–18]. Controlled doping gradients [19, 20] provide an alternate way of introducing unconventional vector potentials. As discussed in greater detail in the following, an additional application of a weak supercurrent provides a simple way to detect the underlying quantum oscillations.

Vector potentials from lattice deformations and doping gradients. —

Consider a prototypical Hamiltonian [21] on the square lattice $\hat{H} = \hat{H}_{TB} + \hat{H}_{\Delta}$ corresponding to a nearest-neighbor

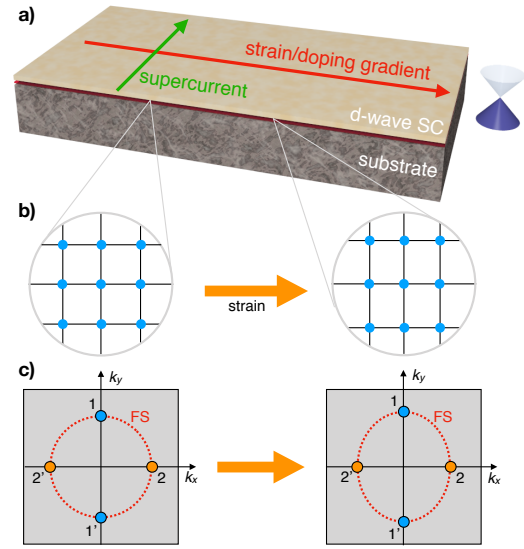


FIG. 1. a) Sketch of a possible experimental setup. The red arrow indicates the direction of variation of either strain or doping gradient. The green arrow indicates an applied supercurrent. Panel (b) shows the schematic deformation of the 2D square lattice for the case of uniaxial strain as a function of x alone. The corresponding Fermi surface (c) deforms and the nodal points, labeled (1,1') and (2,2'), move, mimicking the action of a pseudo-vector potential.

(NN) tight-binding (TB) part, together with a pairing potential at mean-field level for next-nearest neighbors (NNN). The latter is chosen to belong to the d_{xy} representation of the D_{4h} point group. In momentum space, the Nambu form of the lattice Hamiltonian is written as $\hat{H} = \sum_{\mathbf{k}} \Psi_{\mathbf{k}}^{\dagger} \mathcal{H}(\mathbf{k}) \Psi_{\mathbf{k}}$ with $\Psi_{\mathbf{k}} = (c_{\mathbf{k},\uparrow}, c_{\mathbf{k},\downarrow}, c_{-\mathbf{k},\uparrow}^{\dagger}, c_{-\mathbf{k},\downarrow}^{\dagger})^T$ the Nambu spinor and

$$\mathcal{H}(\mathbf{k}) = h_{\mathbf{k}} \sigma_0 \tau_z + \Delta_{\mathbf{k}} (i\sigma_y)(i\tau_y). \quad (1)$$

Here σ and τ are Pauli matrices in spin and Nambu space, respectively, $h_{\mathbf{k}} = 2t[\cos(k_x a) + \cos(k_y a)] - \mu$ and $\Delta_{\mathbf{k}} = 4\Delta \sin(k_x a) \sin(k_y a)$. In addition, t , Δ are the unperturbed hopping coefficients and pairing amplitudes, respectively, and

a is the pristine NN lattice spacing.

In the absence of any perturbation and below half-filling, the low-energy spectrum of \hat{H} is Dirac-like

$$E_{\mathbf{q}}^{(\alpha)} = \pm \sqrt{v_F^2 q_{x/y}^2 + v_{\Delta}^2 q_{y/x}^2}, \quad (2)$$

about four nodes located at $\mathbf{K}_{\alpha} \in \{(\pm K_F, 0), (0, \pm K_F)\}$, where K_F is the Fermi wavevector. We label the pairs of opposite momenta as $\alpha \in \{1, 1'\}$ for the nodes along the k_y axis and $\alpha \in \{2, 2'\}$ for the nodes along the k_x axis in the Brillouin Zone, as shown in Fig. 1 (c). We also define the effective Fermi velocities $v_F = 2ta \sin(K_F a)$, $v_{\Delta} = 4\Delta a \sin(K_F a)$.

We model an arbitrary lattice deformation via the transformation

$$\mathbf{R}_i \rightarrow \mathbf{R}'_i = \mathbf{R}_i + \boldsymbol{\epsilon}(\mathbf{R}_i), \quad (3)$$

where \mathbf{R}_i are Bravais lattice vectors and $\boldsymbol{\epsilon}(\mathbf{R}_i)$ are position-dependent displacements of the orbitals. We assume that both NN hopping coefficients and NNN pairing amplitudes are continuous functions of the deformation. While in practice they can be quite sensitive to the details of the material at hand, we assume that the effect of a deformation can be generically modeled by considering the leading contributions in a gradient expansion of a deformation field $\boldsymbol{\epsilon}(\mathbf{r})$. In addition, we also assume that the leading effect can be captured by a net change in NN bond length, by analogy with the case of graphene [22, 23]. We also ignore the contributions from the change in pairing, which are expected to be sub-leading. While we expect that none of these approximations are crucial for the study of the effect at hand, they provide for a much more transparent discussion.

The pairing potential connects states in the vicinity of pairs of opposite Fermi wavevectors. Consequently, we can focus on the $(1, 1')$ pair of nodes. In the low-energy, continuum limit, the Hamiltonian reduces to $H^{(1,1')} = \int d^2r \Psi_{\mathbf{r}}^{\dagger} \mathcal{H} \Psi_{\mathbf{r}}$, with

$$\mathcal{H} = v_F \left(\sigma_z \tau_0 i \partial_y + \sigma_0 \tau_z \frac{e \mathcal{A}_y}{v_F} \right) - v_{\Delta} \sigma_x \tau_x i \partial_x, \quad (4)$$

where \hbar has been set to 1 for simplicity. A detailed derivation of this Hamiltonian is provided in the Supplementary Material (SM) but the origin of the vector potential can be understood intuitively by inspecting Fig. 1(b,c). Note that $\boldsymbol{\sigma}$ are now Pauli matrices in *combined* valley and spin space, and $\Psi_{\mathbf{r}} = (\Psi_{\uparrow}^{(1)}, \Psi_{\downarrow}^{(1')}, \Psi_{\uparrow}^{(1)\dagger}, \Psi_{\downarrow}^{(1')\dagger})$ is the corresponding Nambu spinor. The Fermi fields are defined for the pristine system in the vicinity of the nodes in standard fashion. Notice that both kinetic and pairing parts are effectively one-dimensional in this limit. Consequently, the deformation-induced potentials, which couple in a gauge-invariant way, are of the form $\mathcal{A} = (0, \mathcal{A}_y)$. The effective one-dimensional form also precludes the emergence of scalar potentials for a generic deformation, in contrast to the case of graphene [8, 24, 25], where this holds only for pure shear deformations. The effective Hamiltonian about the other two Fermi wavevectors can be obtained by transforming $x \leftrightarrow y$.

Under our assumptions, the generic form of the vector potentials are (SM)

$$\mathcal{A}_y = \left(\frac{2t\beta}{e} \right) [u_{xx} + \cos(K_F a) u_{yy}], \quad (5)$$

where $u_{ij} = (1/2)(\partial_j \epsilon_i + \partial_i \epsilon_j)$ is a symmetric strain tensor and $\beta = d \ln t / d \ln a$ is a standard parameter [23]. Quite generally, the elements of the strain tensor can be continuous functions of (x, y) . We list three limiting cases, which are more conveniently achieved, in numerical calculations and possible experimental setups: (i) *Uniaxial strain*, $u_{xx} \neq 0$, $u_{yy} = 0$; (ii) *Hydrostatic compression/dilation*, $u_{xx} = u_{yy}$; and (iii) *Pure shear strain*, $u_{xx} = -u_{yy}$. In the following, we shall focus on case (iii), although this does not essentially modify the results.

A very similar form is obtained for the case of a doping gradient in the low-energy limit. This possibility can be modeled by introducing a slow variation of the chemical potential on the scale of the inter-site separation. In the low-energy, continuum limit we approximate $\mu \rightarrow \mu(1 + g(\mathbf{r}))$. As for the case of lattice deformations, the additional term leads to the emergence of vector potentials of the form

$$\mathcal{A}_y = \left(\frac{\mu}{e} \right) g(\mathbf{r}). \quad (6)$$

This again can be understood intuitively by noting that doping gradient changes the Fermi surface volume and thus moves the nodal points in the momentum space.

The vector potentials in Eqs. 5 and 6 can lead to pseudo-magnetic fields, provided that $\mathcal{B} = \nabla \times \mathcal{A} \neq 0$. In practice, we analyze the case of strains with monotonic linear variation with distance along x and analogously for the chemical potential case. This corresponds to uniform pseudo-magnetic fields. To ensure that the continuum limit is a good approximation to the perturbed finite-size system, we require that the components of the vector potentials remain small over the entire sample.

The vector potential terms are invariant under the time-reversal operation, which effectively interchanges the valley and spin indices of the paired fields. Consequently, the Hamiltonian in Eq. 4 is also invariant under time-reversal. This ensures that the current density associated with either the deformation or doping gradient vanishes. An important consequence of this is the absence of screening currents and hence of the Meissner effect, which would otherwise prevent the emergence of Landau levels (LL). We also note that, from a generic Landau-Ginzburg perspective, there is no analog for the standard London equations as the effective strain-induced vector potentials are not determined from the standard gauge-invariant action. Instead, they are derived from a linear-elastic theory, as noted in the case of graphene [23]. Similar arguments hold for doping gradient-induced vector potentials.

The solutions to Eq. 4 can be obtained via a canonical Bogoliubov-de Gennes (BdG) transformation [2]. For node

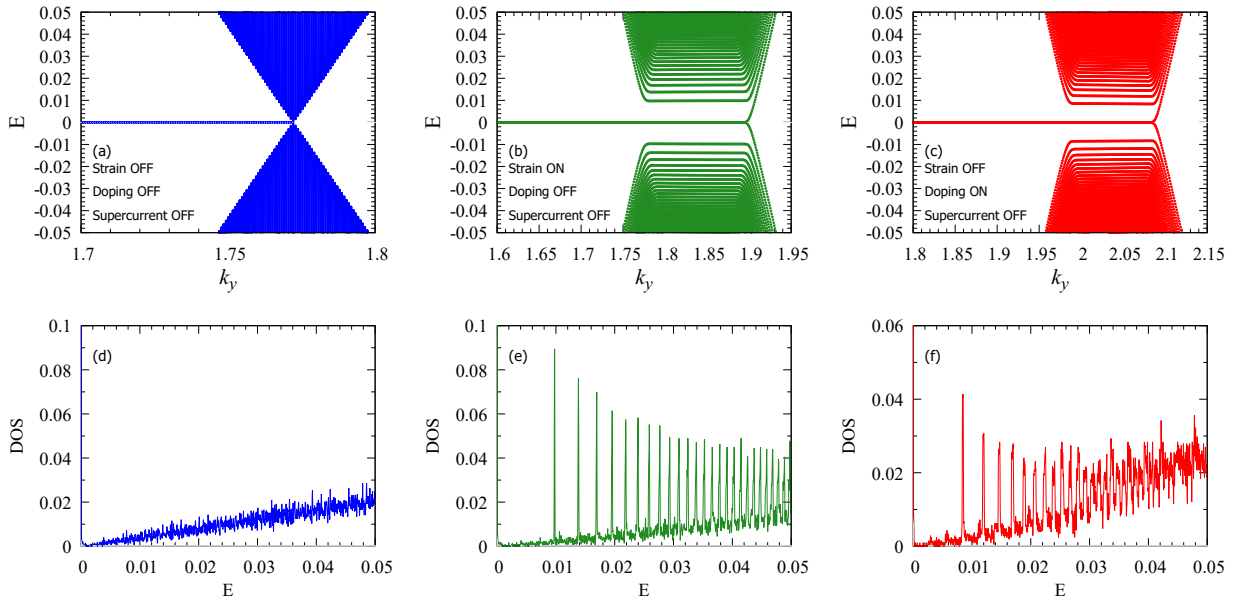


FIG. 2. Results of the numerical calculations for the 2D d_{xy} SC with and without the presence of strain and doping gradients. Computations were performed on a lattice with $L_x = 2000$ sites and $L_y = 8000$ crystal momentum points. We use $\Delta = 0.1$, and $\mu = -1.6$ and $\mu = -1.0$ for the strain and doping cases, respectively. (a) Low-energy spectrum around node 1 in the absence of either strain or doping gradients. (b) Same as in (a) with a finite pure-shear strain with $\delta_{sp} = 5 \times 10^{-5}$ which varies along the x -direction. (c) Same as in (b) with a doping gradient $\delta_{dp} = 1 \times 10^{-4}$ instead of strain. (d)-(f) The total DOS per unit area for the cases in (a)-(c) respectively.

1 the BdG equations are

$$-\left(v_{\Delta} i \partial_x \sigma_x + v_F \left(i \partial_y + \frac{e A_y}{v_F}\right) \sigma_y\right) \psi = E \psi, \quad (7)$$

where σ are Pauli matrices and $\psi = (u_E^{(1)}(\mathbf{r}), v_E^{(1)}(\mathbf{r}))^T$ is a spinor associated with the BdG factors. For A_y linearly increasing along x the eigenstates are discrete Landau levels of energy $E_n = \pm \omega_c \sqrt{n}$, where $\omega_c = \sqrt{2e v_{\Delta} \partial_x A_y(x)}$. The eigenstates at $1'$ are obtained via complex-conjugation.

For *bona fide* magnetic fields it is well-known [7] that Landau quantization generically leads to oscillations in thermodynamic and transport observables with applied field, most notably the de Haas-van Alphen and Shubnikov-de Haas effects. Similar effects have been predicted for strain-induced pseudo-magnetic fields in Dirac [8] and Weyl materials [15]. These oscillations can be traced [7] to the dramatic enhancements in the total density of states (DOS) per unit volume whenever a LL crosses the Fermi energy. We argue that similar singularities arise in the present case, and that the associated oscillations can be observed in principle in a suitable experimental setup. In the case of a clean superconductor under strain or doping gradient, a convenient way to probe the discrete nature of the LL's is to apply a small supercurrent to the sample as indicated in Fig. 1 (a). In the low-energy limit, the supercurrents induce an effective Doppler shift in quasiparticle energy [3] given by $E_{\mathbf{k}} \rightarrow E_{\mathbf{k}} + \mathbf{v}_s \cdot \mathbf{k}$ where $\mathbf{v}_s = \mathbf{q}_s/m$ defines the superfluid velocity [2]. This perturbation breaks time-reversal symmetry and, importantly, leads to opposite shifts around op-

posite momenta. We argue that this effect also occurs in the presence of strains or doping gradients. For fixed effective vector potentials, the DOS at the Fermi level will therefore exhibit sharp enhancements as a function of a weak, applied supercurrent. Similar effects are expected in the presence of fixed supercurrents and varying strain or doping gradients. In the following, we present numerical calculations which fully support our predictions.

Numerical Results. – We model the lattice under strain via a slow variation of the hopping coefficients on the scale of the inter-site spacing. For convenience, we consider pure shear strain as a function of x alone. The hopping coefficients are modulated as $t \rightarrow t(1 \pm l \delta_{sp})$, along x and y -direction respectively, where l denotes the position along x , and δ_{sp} is a small parameter. In the case of doping gradients we allow the chemical potential to vary as $\mu \rightarrow \mu(1 + l \delta_{dp})$, as a function of the x -coordinate alone. Consequently, we impose periodic and open boundary conditions along the y - and x -axes respectively. In the low-energy limit the modified coefficients lead to vector potentials (Eqs. 5, 6), corresponding to uniform pseudo-magnetic fields only around the $(1, 1')$ pair of nodes. For an expanded discussion, please consult the SM.

We find the energy spectra of the modified lattice Hamiltonians numerically. All results are reported in units where $ta = 1$. The largest change in either hopping or chemical potential over the entire extent of the lattice is on the order of 10%.

In Fig. 2 (a) we show the low-energy spectrum as a func-

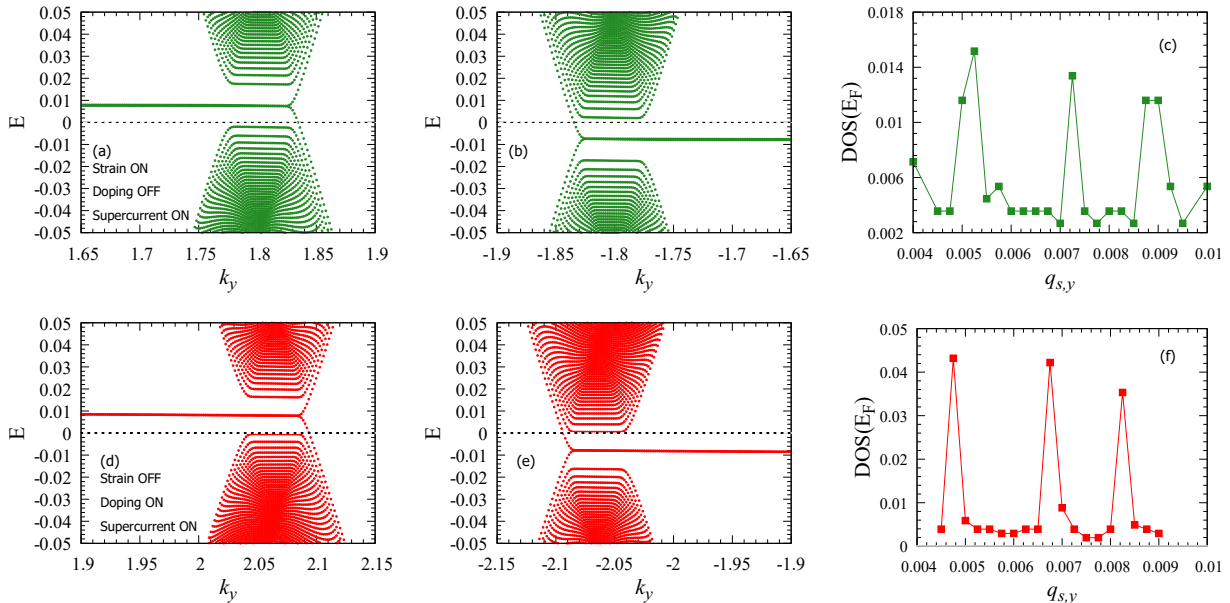


FIG. 3. Results of the numerical calculations for the 2D d_{xy} SC in the presence of strain and doping gradient and of an applied supercurrent. (a) The low-energy spectrum around node 1 in the presence of strain and of an applied supercurrent in the y -direction. (b) Same as (a) for the opposite node $1'$. Note that the LL's have an opposite shift in energy w.r.t. node 1. (c) The DOS at the Fermi level E_F as a function of the applied supercurrent parameterized by the effective momentum $q_{s,y}$ [2]. The sharp spikes occur whenever a pair of LL's crosses the Fermi energy. (d)-(f) Same as (a)-(c) in the presence of a doping gradient alone.

tion of k_y for the unperturbed d_{xy} superconductor around the node 1. Note that the presence of the flat zero-energy dispersion is associated with topologically-protected Majorana edge states [27] and is unrelated to the effect under discussion. In the presence of strain, the low-energy spectrum around the $(1, 1')$ pair of nodes is re-organized into discrete, flat bands as illustrated in Fig. 2 (b). The inter-level energy differences are those predicted by the Dirac-Landau spectrum. Similar effects are observed upon the inclusion of a weakly-varying chemical potential as shown in Fig. 2 (c). The associated total DOS per unit area in the low-energy sectors, Figs. 2 (d)-(f), reflects the emergence of LL's.

In the presence of both strain and weak, applied supercurrents the spectrum around the opposite $(1, 1')$ points is shifted to higher and lower energies respectively, as shown in Figs. 3 (a) and (b). An analogous behavior is obtained in the case of a doping gradient, as shown in Figs. 3 (d) and (e). The total DOS per unit area in the presence of an applied supercurrent reflects the shifts in energies of the LL's. Most notably, it exhibits sharp enhancements whenever pairs of LL's around opposite nodes cross the Fermi energy. This is shown in Figs. 3 (c) and (f) for a range of supercurrents for strain and doping gradient cases, respectively. Note that the applied supercurrent also lifts the degeneracy of the LL's and leads to a broadening of the sharp peaks in the DOS.

Summary and outlook. – We proposed that weak, slowly-varying strains and doping gradients generically give rise to pseudo-magnetic fields in the low-energy limit of two-

dimensional nodal superconductors. For simplicity, our discussion was focused on a prototypical 2D d_{xy} SC. This is not essential and similar effects are expected to occur in other types of SC which exhibit Dirac-like spectra around points in the Brillouin Zone. Examples include $d_{x^2-y^2}$ cuprates and odd-parity p -wave cases. In view of similar proposals for pseudo-magnetic fields in Weyl semi-metals [10–15, 28], such effects are also likely to occur in more complicated 3D systems.

The most likely candidates for the experimental observation of such effects are high- T_c cuprates. Specifically, in $\text{YBa}_2\text{Cu}_3\text{O}_x$ thin films and $\text{La}_{2-x}\text{Sr}_x\text{CuO}_4$ - La_2CuO_4 bilayer samples controlled doping gradients have recently been achieved [19, 20]. According to our theory such samples should already exhibit Landau level quantization which is in principle observable as a series of sharp peaks in DOS through standard quasiparticle spectroscopies such as the angle-resolved photoemission (ARPES) or scanning tunneling spectroscopy (STS). In the above samples a $\sim 10\%$ doping change is imposed over a millimeter scale which allows us to estimate (SM) the effective pseudo-magnetic field as $\mathcal{B} \simeq 0.32$ mT and the Landau level spacing $\hbar\omega_c \simeq 82$ μeV . While this is probably too small to resolve by STS or ARPES we see no fundamental reason why similar doping variations could not be imposed on a μm scale which would produce an effective field of order one Tesla and clearly observable Landau levels. Under the applied supercurrent such samples would in addition show quantum oscillations in transport

properties, such as the longitudinal thermal conductivity κ_{xx} . We speculate that they might also exhibit exactly quantized thermal Hall conductance κ_{xy} when the zero of the energy is tuned to lie between the bulk Landau levels by supercurrent as in Fig. 3 and the electronic contribution to κ_{xx} vanishes. In this situation each bulk band is expected to carry a nonzero Chern number and produce a protected chiral edge mode, already visible in Fig. 3 as a dispersing feature terminating the flat Landau levels. Finally, large local strain gradients have recently been observed in nanocomposite $\text{YBa}_2\text{Cu}_3\text{O}_{7-\delta}$ films [18] which may afford an opportunity to study the effects discussed in this paper on nanoscale, similar to the seminal work on “nanobubbles” in graphene [9].

During the preparation of this manuscript, we became aware of the similar results reported in Ref. [29].

Acknowledgements. – The authors are indebted to T. Liu for illuminating discussions and thank NSERC, CIFAR and Max Planck - UBC Centre for Quantum Materials for support.

* Corresponding author: enica@qmi.ubc.ca

- [1] J. Bardeen, L. N. Cooper, and J. R. Schrieffer, *Phys. Rev.* **106**, 162 (1957).
- [2] P. G. de Gennes, *Superconductivity of metals and alloys* (Westview Press, 1999).
- [3] M. Tinkham, *Introduction to superconductivity* (McGraw-Hill, N. Y. , 1996).
- [4] W. Meissner, and R. Ochsenfeld, *R., Naturwissenschaften.* **21** (44), 787 (1933).
- [5] A. A. Abrikosov, *Soviet Physics JETP* **5**, 1174 (1957).
- [6] M. Franz and Z. Tesanovic, *Phys. Rev. Lett.* **84**, 554 (2000).
- [7] D. Shoenberg, *Magnetic Oscillations in Metals* (Cambridge University Press, Cambridge, 1984).
- [8] F. Guinea, M. I. Katsnelson, and A. K. Geim, *Nat. Phys.* **6**, 30 (2009).
- [9] N. Levy *et al*, *Science* **329**, 544 (2010).
- [10] H. Shapourian, T. L. Hughes, and S. Ryu, *Phys. Rev. B* **92**, 165131 (2015).
- [11] A. Cortijo, Y. Ferreiros, K. Landsteiner, and M. A. H. Vozmediano, *Phys. Rev. Lett.* **115**, 177202 (2015).
- [12] H. Sumiyoshi and S. Fujimoto, *Phys. Rev. Lett.* **116**, 166601 (2016).
- [13] D.I. Pikulin, Anffany Chen, and M. Franz, *Phys. Rev. X* **6**, 041021 (2016).
- [14] A. G. Grushin, J. W.F. Venderbos, A. Vishwanath, and R. Ilan, *Phys. Rev. X* **6**, 041046 (2016).
- [15] T. Liu, D. I. Pikulin, and M. Franz, *Phys. Rev. B* **95**, 041201(R) (2017).
- [16] I. Bozovic, G. Logvenov, I. Belca, B. Narimbetov, and I. Sveklo *Phys. Rev. Lett.* **89**, 107001 (2002).
- [17] A. Chen *et al.*, *Sci. Adv.* **2**, e1600245 (2016).
- [18] R. Guzman, J. Gazquez, B. Mundet, M. Coll, X. Obradors, and T. Puig, *Phys. Rev. Materials* **1**, 024801 (2017).
- [19] B. J. Taylor *et al*, *Phys. Rev. B*, **91**, 144511 (2015).
- [20] J. Wu *et al*, *Nat. Mater.* **12**, 877 (2013).
- [21] S.H. Simon and P.A. Lee *Phys. Rev. Lett.* **78**, 1548 (1997).
- [22] H. Suzuura and T. Ando, *Phys. Rev. B* **65**, 235412 (2002).
- [23] M. A. H. Vozmediano, M. I. Katsnelson, and F. Guinea, *Phys. Rep.* **496**, 109 (2010).
- [24] J. L. Manes, *Phys. Rev. B* **76**, 045430 (2007).
- [25] J. L. Manes, F. de Juan, M. Sturla, and M. A. H. Vozmediano, *Phys. Rev. B* **88**, 155405 (2013).
- [26] K.-I. Sasaki, Y. Kawazoe, and R. Saito, *Prog. Theor. Phys.* **113**, 463 (2005).
- [27] A. C. Potter and P. A. Lee, *Phys. Rev. Lett.* **112**, 11702 (2014).
- [28] T. Liu, M. Franz and S. Fujimoto, (unpublished).
- [29] G. Massarelli, G. Wachtel, J. Y. T. Wei, A. Paramakanti, arXiv:1707.07683.

Landau levels from neutral Bogoliubov particles in two-dimensional nodal superconductors under strain and doping gradients :

Supplementary Material

In Sec. I (a) and (b) we define the lattice pairing Hamiltonian and derive the effect of an arbitrary but slowly-varying deformation in the low-energy, continuum limit. In Sec. I (c) we give the most general expression for the resulting vector potentials. The analogous case of a doping gradient is briefly discussed in Sec. I (d). In Sec. I (e), we write the explicit form of the low-energy Hamiltonian (Eq. 4 of the main text). The effective lattice models used in the numerical calculations are discussed in Sec. II. Finally, Sec. III gives the estimates for the LL spacing and pseudo-magnetic fields reported in the main text.

I. LOW-ENERGY, CONTINUUM LIMIT IN THE PRESENCE OF ARBITRARY DEFORMATIONS AND DOPING GRADIENTS

The Hamiltonian on the two-dimensional square lattice is given by

$$\hat{H} = \hat{H}_{TB} + \hat{H}_{\Delta} \quad (S1)$$

where \hat{H}_{TB} is a nearest-neighbor (NN) tight-binding part, and \hat{H}_{Δ} is a pairing part corresponding to a d_{xy} irreducible representation of the D_{4h} point group.

a. Tight-binding part in the presence of an arbitrary deformation

In the absence of strain, the TB part is given by

$$\hat{H}_{TB} = \sum_i \left[\sum_{j \in \langle ij \rangle} \sum_{\sigma} t(\delta_j) c_{\sigma}^{\dagger}(\mathbf{R}_i) c_{\sigma}(\mathbf{R}_i + \delta_j) + h.c. \right] - \sum_i \mu c_{\sigma}^{\dagger}(\mathbf{R}_i) c_{\sigma}(\mathbf{R}_i), \quad (S2)$$

where σ is a spin index which is ignored for the rest of this subsection. \mathbf{R}_i are the Bravais lattice vectors, while $\delta_j \in \{(a, 0), (0, a)\}$ are the vectors which connect NN's, a is the NN distance, and μ is the chemical potential. The latter is chosen s.t. the system is below half-filling. \hat{H}_{TB} can be diagonalized by applying a Fourier transform

$$c(\mathbf{R}_i) = \frac{1}{\sqrt{N}} \sum_{\mathbf{k} \in BZ} e^{i\mathbf{k} \cdot \mathbf{R}_i} c_{\mathbf{k}}, \quad (S3)$$

where N is the number of unit cells.

In the presence of a lattice deformation, the lattice TB Hamiltonian undergoes the transformation

$$\mathbf{R}_i \rightarrow \mathbf{R}'_i = \mathbf{R}_i + \epsilon(\mathbf{R}_i), \quad (S4)$$

where $\epsilon(\mathbf{R}_i)$ is a position-dependent displacement. In general, the hopping coefficients are modified accordingly:

$$\begin{aligned} t(\delta_j) \rightarrow t'(\delta_j) &= t[\mathbf{R}_i + \delta_j + \epsilon(\mathbf{R}_i + \delta_j) - \mathbf{R}_i - \epsilon(\mathbf{R}_i)] \\ &= t[\delta_j + \epsilon(\mathbf{R}_i + \delta_j) - \epsilon(\mathbf{R}_i)]. \end{aligned} \quad (S5)$$

We assume that the hopping coefficients can be approximated by continuous functions of the displacement. The transformed Hamiltonian is

$$\begin{aligned} \hat{H}_{TB} \rightarrow \hat{H}'_{TB} &= \sum_i \left[\sum_{j \in \langle ij \rangle} t[\delta_j + \epsilon(\mathbf{R}_i + \delta_j) - \epsilon(\mathbf{R}_i)] c^{\dagger}(\mathbf{R}_i + \epsilon(\mathbf{R}_i)) c(\mathbf{R}_i + \epsilon(\mathbf{R}_i + \delta_j) + \delta_j) + h.c. \right] \\ &\quad - \sum_i \mu c^{\dagger}(\mathbf{R}_i + \epsilon(\mathbf{R}_i)) c(\mathbf{R}_i + \epsilon(\mathbf{R}_i)). \end{aligned} \quad (S6)$$

We consider the low-energy, continuum limit of \hat{H}'_{TB} . Consequently, we approximate the lattice operators as products of parts which vary rapidly and slowly on the scale of the lattice as

$$c(\mathbf{R}_i) \approx \sum_{\alpha} e^{i\mathbf{K}_{\alpha} \cdot \mathbf{R}_i} \Psi^{(\alpha)}(\mathbf{R}_i), \quad (S7)$$

where $\Psi^{(\alpha)}(\mathbf{R}_i)$ is a slowly-varying Fermi field and $\alpha \in \{1, 1', 2, 2'\}$ represents the positions of the four nodes at Fermi wave-vectors $\mathbf{K}_\alpha \in \{(0, \pm K_F), (\pm, K_F, 0)\}$. We assume that the lattice displacements can be approximated by a continuous displacement field:

$$\mathbf{R}_i + \epsilon(\mathbf{R}_i) \rightarrow \mathbf{r} + \epsilon(\mathbf{r}). \quad (\text{S8})$$

On the scale of the lattice, variations in the displacements can be approximated by

$$\epsilon(\mathbf{r} + \delta_j) \approx \epsilon(\mathbf{r}) + (\delta_j \cdot \nabla)\epsilon(\mathbf{r}). \quad (\text{S9})$$

In the following, we expand the continuum limit of the Hamiltonian in terms of leading gradient terms.

It should be noted that such an expansion is valid provided that the gradient term in Eq. S9 remains small throughout. As discussed in the following, in order to obtain finite pseudo-magnetic fields we consider deformation gradients which vary monotonically. This implicitly introduces a spatial scale at which these gradients are no longer small. Therefore, the effective continuum approximation only holds provided that the deformation at any point of a sample of finite extent remains small.

Applying the above to \hat{H}_{TB} , we obtain

$$\begin{aligned} \hat{H}'_{TB} = & \int d^2r \sum_{\alpha} \Psi^{\dagger,(\alpha)}(\mathbf{r} + \epsilon) \left\{ \sum_j 2t \left(\delta_j + (\delta_j \cdot \nabla)\epsilon \right) \left[\cos \left(\mathbf{K}_\alpha \cdot (\delta_j + (\delta_j \cdot \nabla)\epsilon) \right) \right. \right. \\ & \left. \left. + i \sin \left(\mathbf{K}_\alpha \cdot (\delta_j + (\delta_j \cdot \nabla)\epsilon) \right) (\delta_j \cdot \nabla) \right] \right\} \Psi^{(\alpha)}(\mathbf{r} + \epsilon) - \mu \sum_{\alpha} \int d^2r \Psi^{\dagger,(\alpha)}(\mathbf{r} + \epsilon) \Psi^{(\alpha)}(\mathbf{r} + \epsilon), \end{aligned} \quad (\text{S10})$$

where we neglected inter-node terms. The explicit dependence of the fields on ϵ can be formally eliminated via a coordinate transformation

$$\mathbf{r}' = \mathbf{r} + \epsilon(\mathbf{r}), \quad (\text{S11})$$

with a Jacobian $1 + \epsilon_{ii}$, where $\epsilon_{ij} = \partial_j \epsilon_i$ and implicit summation is assumed. We also approximate $\delta_j \cdot \nabla \epsilon(\mathbf{r}) \approx \delta_j \cdot \nabla \epsilon(\mathbf{r}')$ and expand the following terms

$$t \left(\delta_j + (\delta_j \cdot \nabla)\epsilon \right) \approx t(\delta_j) + (\delta_j \cdot \nabla)\epsilon \cdot \nabla t(\delta_j), \quad (\text{S12})$$

$$\cos \left(\mathbf{K}_\alpha \cdot (\delta_j + (\delta_j \cdot \nabla)\epsilon) \right) \approx \cos(\mathbf{K}_\alpha \cdot \delta_j) - \mathbf{K}_\alpha \cdot (\delta_j \cdot \nabla)\epsilon \sin(\mathbf{K}_\alpha \cdot \delta_j), \quad (\text{S13})$$

$$\sin \left(\mathbf{K}_\alpha \cdot (\delta_j + (\delta_j \cdot \nabla)\epsilon) \right) \approx \sin(\mathbf{K}_\alpha \cdot \delta_j) + \mathbf{K}_\alpha \cdot (\delta_j \cdot \nabla)\epsilon \cos(\mathbf{K}_\alpha \cdot \delta_j). \quad (\text{S14})$$

To zeroth order in the gradient expansion we obtain

$$\begin{aligned} H_{TB}^{(0)} = & \int d^2r \sum_{\alpha} \sum_j 2t(\delta_j) \Psi^{\dagger,(\alpha)}(\mathbf{r}) \left\{ \cos(\mathbf{K}_\alpha \cdot \delta_j) + i \sin(\mathbf{K}_\alpha \cdot \delta_j) (\delta_j \cdot \nabla) \right\} \Psi^{(\alpha)}(\mathbf{r}) \\ & - \mu \sum_{\alpha} \int d^2r \Psi^{\dagger,(\alpha)}(\mathbf{r}) \Psi^{(\alpha)}(\mathbf{r}). \end{aligned} \quad (\text{S15})$$

The first and last terms cancel, since \mathbf{K}_α is on the Fermi surface. The second term gives the leading linear dispersion and also defines the Fermi velocity $v_F = 2ta \sin(K_F a)$.

To first order, we obtain

$$\begin{aligned} H_{TB}^{(1)} = & \sum_{\alpha} \sum_j \left\{ \int d^2r (\epsilon_{xx} + \epsilon_{yy}) 2t(\delta_j) \cos(\mathbf{K}_\alpha \cdot \delta_j) + \int d^2r 2(\delta_j \cdot \nabla)\epsilon \cdot \nabla t \cos(\mathbf{K}_\alpha \cdot \delta_j) \right. \\ & \left. + \int d^2r 2t(\delta_j) (-\mathbf{K}_\alpha \cdot (\delta_j \cdot \nabla)\epsilon \sin(\mathbf{K}_\alpha \cdot \delta_j)) \right\} \Psi^{\dagger,(\alpha)}(\mathbf{r}) \Psi^{(\alpha)}(\mathbf{r}) \\ & - \mu \sum_{\alpha} \int d^2r (\epsilon_{xx} + \epsilon_{yy}) \Psi^{\dagger,(\alpha)}(\mathbf{r}) \Psi^{(\alpha)}(\mathbf{r}). \end{aligned} \quad (\text{S16})$$

The first two terms cancel independently of the details of the deformation. These represent a local dilation/contraction with all other parameters fixed. The expression can be simplified further by carrying out the summations over NN's. The result is summarized by

$$H_{TB}^{(1)} = \sum_{\alpha} \int d^2r e \mathcal{A}^{\alpha}(\mathbf{r}) \Psi^{\dagger,(\alpha)}(\mathbf{r}) \Psi^{(\alpha)}(\mathbf{r}), \quad (\text{S17})$$

where the electron charge e was introduced for dimensional consistency. The effective *vector* potentials around either $(1, 1')$ nodes are defined as

$$\mathcal{A}^{(1,1')} = \begin{pmatrix} 0 \\ \left(\frac{2a}{e} \left[t'_{\parallel} \epsilon_{xx} + t'_{\perp} \epsilon_{yx} + t'_{\perp} \cos(K_F a) \epsilon_{xy} + \left(t'_{\parallel} \cos(K_F a) - t K_F \sin(K_F a) \right) \epsilon_{yy} \right] \right) \end{pmatrix} \quad (\text{S18})$$

The \mathcal{A}_x component is formally set to zero since there is no linear-derivative term along the x -direction to leading order for the TB part. We also defined the coefficients $\partial_x t_x = \partial_y t_y = t'_{\parallel}$, $\partial_x t_y = \partial_y t_x = t'_{\perp}$, which are restricted by the symmetry of the square lattice, while, in general, $t'_{\perp} \neq t'_{\parallel}$. The analogous non-trivial vector potentials \mathcal{A}_x around the other pair of Fermi momenta can be obtained by replacing $x \leftrightarrow y$.

b. Pairing part in the presence of an arbitrary deformation

In the absence of any deformation, the pairing part of the Hamiltonian for a 2D d_{xy} SC is given by

$$\hat{H}_{\Delta} = \sum_i \sum_{j \in \langle\langle ij \rangle\rangle} \sum_{\sigma} \sum_{\sigma'} \Delta_{\sigma\sigma'}(\delta_j) [c_{\sigma}(\mathbf{R}_i) c_{\sigma'}(\mathbf{R}_i + \delta_j) + c_{\sigma}(\mathbf{R}_i) c_{\sigma'}(\mathbf{R}_i - \delta_j)] + h.c., \quad (\text{S19})$$

where the pairing occurs for next-nearest neighbor (NNN) sites, $\Delta_{\sigma\sigma'}(\delta_j) = \Delta(\delta_j) i\sigma_y$ corresponding to even-parity, spin-singlet pairing. In addition, $\Delta(\delta_{1/2}) = \pm\Delta$, with $\delta_{1/2} = (\pm a, a)$ determining the vectors which connect NNN's.

We allow for the deformation given by Eq. S8 and assume that its effect on the pairing potential can be generically captured to lowest order in the strains. The derivation of the low-energy, continuum limit is analogous to that of the TB part. We list the final results for the $(1, 1')$ pair of nodes:

$$H_{\Delta}^{(0)} = \int d^2r \sum_{(\alpha,\beta)} 4a \Delta_{\sigma\sigma'} \sin(K_{Fy,\alpha} a) \Psi_{\sigma}^{\alpha}(\mathbf{r}) (-i\partial_x) \Psi_{\sigma'}^{\beta}(\mathbf{r}) + h.c., \quad (\text{S20})$$

$$H_{\Delta}^{(1)} = \int d^2r \sum_{(\alpha,\beta)} \sum_{\sigma,\sigma'} (-i\sigma_y)_{\sigma,\sigma'} 4a \left[(\epsilon_{xx} \partial_x \Delta + \epsilon_{yx} \partial_y \Delta) \cos(K_F a) - \Delta K_F \epsilon_{yx} \sin(K_F a) \right] \Psi_{\sigma}^{\alpha}(\mathbf{r}) \Psi_{\sigma'}^{\beta}(\mathbf{r}), \quad (\text{S21})$$

where $\alpha \neq \beta$. The zeroth-order term defines a velocity $v_{\Delta} = 4a\Delta \sin(K_F a)$. For the $(2, 2')$ pair, we replace $x \leftrightarrow y$. We can also set $\partial_x \Delta = \partial_y \Delta = \Delta'$.

c. Effective gauge potentials in the presence of strain

The first-order corrections to the pairing part can be eliminated via the gauge transformation

$$\Psi_{\sigma'}^{\beta} \rightarrow \Psi_{\sigma'}^{\beta} e^{-i \text{sgn}(K_{Fy,\alpha}) \frac{\phi(\mathbf{r})}{v_{\Delta}}}, \quad (\text{S22})$$

where

$$\phi = 4a\Delta' (\epsilon_x + \epsilon_y) \cos(K_{F,\alpha} a) - \Delta K_F \epsilon_y \sin(K_F a). \quad (\text{S23})$$

The transformation modifies \mathcal{A}_y in Eq. S18 to

$$\mathcal{A}'_y = \mathcal{A}_y - \frac{v_F}{v_{\Delta} e} \partial_y \phi. \quad (\text{S24})$$

The terms proportional to $\sin(K_F a)$ cancel. The expression for the most general gauge strain-induced vector potentials for the $(1, 1')$ fields reduces to

$$\mathcal{A}_y = \left(\frac{2a}{e}\right) \left\{ t'_{\parallel} \epsilon_{xx} + \left[t'_{\parallel} - \left(\frac{t}{\Delta}\right) \Delta' \right] \cos(K_F a) \epsilon_{yy} + t'_{\perp} \epsilon_{yx} + \left[t'_{\perp} - \left(\frac{t}{\Delta}\right) \Delta' \right] \cos(K_F a) \epsilon_{xy} \right\}. \quad (\text{S25})$$

The corresponding \mathcal{A}_x for the $(2, 2')$ pair is obtained by replacing $x \leftrightarrow y$. Note that t'_{\parallel} corresponds to a change in bond length, t'_{\perp} to a change change in bond angle, while Δ' includes both. In the most general case, the coefficients depend on the details of the model, and in particular on the symmetry of the orbitals.

We focus on cases where the dominant contribution comes from the change in bond length i.e. $t'_{\parallel} \neq 0, t'_{\perp} \approx 0$. Such an approximation can be justified in principle using a Slater-Koster scheme [S2], and is consistent with the similar case of graphene [S5]. Additionally, we assume that the leading change in the pairing potential under strain Δ is also negligible. Under these assumptions, and writing

$$at'_{\parallel} = t \frac{d \ln t}{d \ln a} = t\beta, \quad (\text{S26})$$

we obtain the form of the vector potentials discussed in the main text.

d. Effective gauge potentials from doping gradients

We consider the effect of a doping gradient $\mu \rightarrow \mu(\mathbf{R}_i)$ on the Hamiltonian of Eq. S1. The low-energy, continuum limit in this case is

$$H = H_{TB}^{(0)} + H_{\Delta}^{(0)} + H_{dg}, \quad (\text{S27})$$

where the first two terms correspond to the unperturbed Hamiltonians for the TB and pairing part, given by Eqs. S15 and S20, respectively. The last term is the contribution of a spatially-varying chemical potential

$$H_{dg} = -e \sum_{\alpha} \int d^2 r \left(\frac{\tilde{\mu}(\mathbf{r})}{e} \right) \Psi^{\dagger,(\alpha)}(\mathbf{r}) \Psi^{(\alpha)}(\mathbf{r}), \quad (\text{S28})$$

where

$$\tilde{\mu}(\mathbf{r}) = \mu g(\mathbf{r}). \quad (\text{S29})$$

The corresponding vector potential around the $(1, 1')$ pair of nodes is

$$\mathcal{A}^{(1,1')} = \begin{pmatrix} 0 \\ \left(\frac{\mu}{e}\right) g(\mathbf{r}) \end{pmatrix}, \quad (\text{S30})$$

with an analogous \mathcal{A}_x around $(2, 2')$. These vector potentials must remain small throughout the finite area of the sample and are subject to the constraints imposed in the case of strain.

e. Low-energy Nambu form of the Hamiltonian in the presence of non-trivial vector potentials

In either strain or doping cases, we can write the Hamiltonian in the low-energy sector as

$$H = \int d^2 r \begin{pmatrix} \Psi_{\uparrow}^{\dagger,(1)} \\ \Psi_{\downarrow}^{\dagger,(1')} \\ \Psi_{\uparrow}^{(1)} \\ \Psi_{\downarrow}^{(1')} \end{pmatrix}^T \begin{pmatrix} v_F \left(i\partial_y + e \frac{\mathcal{A}_y}{v_F} \right) & 0 & 0 & v_{\Delta}(-i\partial_x) \\ 0 & v_F \left(-i\partial_y + e \frac{\mathcal{A}_y}{v_F} \right) & v_{\Delta}(-i\partial_x) & 0 \\ 0 & v_{\Delta}(-i\partial_x) & v_F \left(i\partial_y - e \frac{\mathcal{A}_y}{v_F} \right) & 0 \\ v_{\Delta}(-i\partial_x) & 0 & 0 & v_F \left(-i\partial_y - e \frac{\mathcal{A}_y}{v_F} \right) \end{pmatrix} \begin{pmatrix} \Psi_{\uparrow}^{(1)} \\ \Psi_{\downarrow}^{(1')} \\ \Psi_{\uparrow}^{\dagger,(1)} \\ \Psi_{\downarrow}^{\dagger,(1')} \end{pmatrix}, \quad (\text{S31})$$

which is identical to Eq. 4 of the main text. With vanishing vector potentials, one can easily check that this is the low-energy, continuum limit of the Hamiltonian of Eq. 1 main text:

$$H = \sum_{\mathbf{k}} \begin{pmatrix} c_{\mathbf{k}\uparrow}^\dagger \\ c_{-\mathbf{k}\downarrow} \end{pmatrix}^T \begin{pmatrix} h_{\mathbf{k}} & \Delta_{\mathbf{k}} \\ \Delta_{\mathbf{k}} & -h_{\mathbf{k}} \end{pmatrix} \begin{pmatrix} c_{\mathbf{k}\uparrow} \\ c_{-\mathbf{k}\downarrow}^\dagger \end{pmatrix} + \begin{pmatrix} c_{\mathbf{k}\downarrow}^\dagger \\ c_{-\mathbf{k}\uparrow} \end{pmatrix}^T \begin{pmatrix} h_{\mathbf{k}} & -\Delta_{\mathbf{k}} \\ -\Delta_{\mathbf{k}} & -h_{\mathbf{k}} \end{pmatrix} \begin{pmatrix} c_{\mathbf{k}\downarrow} \\ c_{-\mathbf{k}\uparrow}^\dagger \end{pmatrix}. \quad (\text{S32})$$

The BdG equations can be obtained in standard fashion by considering the block Hamiltonian

$$H' = \int d^2r \begin{pmatrix} \Psi_{\downarrow}^{\dagger,(1')} \\ \Psi_{\uparrow}^{(1)} \end{pmatrix}^T \begin{pmatrix} v_F \left(-i\partial_y + e\frac{A_y}{v_F} \right) & v_{\Delta}(-i\partial_x) \\ v_{\Delta}(i\partial_x) & v_F \left(i\partial_y - e\frac{A_y}{v_F} \right) \end{pmatrix} \begin{pmatrix} \Psi_{\downarrow}^{(1')} \\ \Psi_{\uparrow}^{\dagger,(1)} \end{pmatrix}, \quad (\text{S33})$$

together with the fact that $\Psi_{\downarrow}^{(1')}$, $\Psi_{\uparrow}^{\dagger,(1)}$ are related through time-reversal. The remaining sector can also be obtained via the same operation.

II. NUMERICAL CALCULATIONS

For the purpose of numerical computation, we introduce position-dependent tight-binding coefficients or chemical potentials at the level of the Hamiltonian in Eq. S1. Moreover, these vary slowly on the scale of the lattice. Depending on the spatial dependence of these parameters, we recover the different cases discussed in the main text.

In practice, we allow a non-trivial spatial variation along the x -direction, but keep periodic boundary conditions along y .

a. Deformation-induced vector potentials

In this case, we choose

$$t(\boldsymbol{\delta}_j) \rightarrow t(\boldsymbol{\delta}_j) \left[1 + f(\mathbf{R}_i, \boldsymbol{\delta}_j) \right]. \quad (\text{S34})$$

In the low-energy continuum approximation, the corrections to the hopping coefficients are analogous to the second term in Eq. S16 which is the contribution of the transformed TB coefficients:

$$H_{TB}^{(1)} = \sum_{\alpha} \sum_j \int d^2r 2t f(\mathbf{r}, \boldsymbol{\delta}_j) \cos(\mathbf{K}_{\alpha} \cdot \boldsymbol{\delta}_j) \Psi^{\dagger,(\alpha)}(\mathbf{r}) \Psi^{(\alpha)}(\mathbf{r}). \quad (\text{S35})$$

We consider the three limiting cases discussed in the main text:

(i) *Uniaxial strain along x axis.* This corresponds to $f(x, \boldsymbol{\delta}_x) \neq 0$, with the component in the y direction equal to 0. The vector potential is $\mathcal{A}_y = tf(x, \boldsymbol{\delta}_x)$ for the $(1, 1')$ pair of nodes, and $\mathcal{A}_y = 0$ for the other pair. On the lattice this amounts to $f(x_l, \boldsymbol{\delta}_x) = l\delta_{sp}$, where $\delta_{sp} \ll 1$.

(ii) *Hydrostatic compression/dilatation.* In this case, the finite vector potentials about each pair of nodes are equal. We take $f(x, \boldsymbol{\delta}_x) = f(x, \boldsymbol{\delta}_y) = f(x)$. The dependence on x alone is purely for computational convenience. The resulting vector potentials are $\mathcal{A}_{x/y} = 2tf(x)(1 + \cos(K_F a))$. On the lattice, we have $f(x_l, \boldsymbol{\delta}_x) = l\delta_{sp}$.

(iii) *Pure shear deformation.* We choose $f(x, \boldsymbol{\delta}_x) = -f(x, \boldsymbol{\delta}_y)$. The vector potentials are $\mathcal{A}_{y/x} = \pm 2tf(x)(1 - \cos(K_F a))$. On the lattice, we have $f(x_l, \boldsymbol{\delta}_x) = l\delta_{sp}$, with a corresponding negative sign for hopping along the y direction.

b. Doping gradient-induced vector potentials

This case is qualitatively similar to that of a deformation, since $\tilde{\mu}(\mathbf{r}) = \mu g(\mathbf{r})$. In practice, we take $g(\mathbf{r}) = g(x)$. On the lattice, this amounts to $g(x_l) = l\delta_{dp}$, with $\delta_{dp} \ll 1$.

III. ESTIMATE OF DOPING GRADIENT-INDUCED LANDAU LEVEL SPACING AND PSEUDO-MAGNETIC FIELDS

We estimate that the candidate cuprate films are generically characterized by the parameters

- 1) $\Delta \approx 30$ meV [S6]
- 2) $a \approx 3.9$ Å.
- 3) $K_F a \approx \pi/2$.
- 4) $t \approx 0.38$ eV [S7].
- 5) $\mu \approx 1.52$ eV as determined from $\mu \approx 2t(1 + \cos(K_F a)) \approx 4t$.

In addition, we estimate $\partial_x g(x) \approx 0.047$ nm⁻¹ from the relative variation in hole concentration $\partial_x g(x) \approx (\Delta p)/(p_0 \Delta x)$ over sample length in Ref. S8. The rate in Ref. S9 is roughly half of this. Upon including factors of \hbar for dimensional consistency we obtain

$$E_{c,\text{Doping}} = \sqrt{8\Delta\mu a(\sin(K_F a))\partial_x g(x)} \quad (\text{S36})$$

$$\mathcal{B}_{\text{Doping}} = \frac{\Phi_0}{2\pi} \frac{\mu\partial_x g}{2ta \sin(K_F a)}, \quad (\text{S37})$$

for the inter-LL spacing and pseudo-magnetic field respectively. Note that $\Phi_0 = hc/e = 4.12 \times 10^5$ TÅ² is the quantum of flux.

* Corresponding author: enica@qmi.ubc.ca

- [S1] L. D. Landau and E. M. Lifshitz, *Theory of elasticity* (Pergamon Press, N. Y. , 1970).
[S2] J. C. Slater and G. F. Koster, Phys. Rev. **94**, 1498 (1954).
[S3] P. G. de Gennes, *Superconductivity of metals and alloys* (Westview Press, 1999).
[S4] G. D. Mahan, *Many-particle physics* (Plenum, N. Y. , 2000).
[S5] A. H. Castro *et al*, Rev. Mod. Phys. **81**, 109 (2009).
[S6] M. Hashimoto *et al*, Nat. Phys. **10**, 483 (2014).
[S7] M. M. Korshunov *et al*, Phys. C **402**, 365 (2004).
[S8] B. J. Taylor *et al*, Phys. Rev. B, **91**, 144511 (2015).
[S9] J. Wu *et al*, Nat. Mater. **12**, 877 (2013).